Scaling laws for harmonically trapped two-species mixtures at thermal equilibrium

Francisco Jauffred,[1] Roberto Onofrio,[2,3] and Bala Sundaram[1]
[1]*Department of Physics, University of Massachusetts, Boston, MA 02125, USA*
[2]*Dipartimento di Fisica e Astronomia "Galileo Galilei," Università di Padova, Via Marzolo 8, Padova 35131, Italy*
[3]*Department of Physics and Astronomy, Dartmouth College, 6127 Wilder Laboratory, Hanover, NH 03755, USA*

(Received 5 October 2018; published 11 February 2019)

We discuss the scaling of the interaction energy with particle numbers for a harmonically trapped two-species mixture at thermal equilibrium experiencing interactions of arbitrary strength and range. In the limit of long-range interactions and weak coupling, we recover known results for the integrable Caldeira-Leggett model in the classical limit. In the case of short-range interactions and for a balanced mixture, numerical simulations show scaling laws with exponents that depend on the interaction strength, its attractive or repulsive nature, and the dimensionality of the system. Simple analytic considerations based on equilibrium statistical mechanics and small interspecies coupling quantitatively recover the numerical results. The dependence of the scaling on interaction strength helps to identify a threshold between two distinct regimes. Our thermalization model covers both local and extended interactions, allowing for interpolation between different systems such as fully ionized gases and neutral atoms, as well as parameters describing integrable and chaotic dynamics.

DOI: 10.1103/PhysRevE.99.022116

I. INTRODUCTION

Thermalization in many-body systems is a topic of broad interest in a variety of contexts including fluids, plasmas, and chemical reaction dynamics. An approach which has been considered of universal character, as it may be used for both classical and quantum systems, is based on a closed Hamiltonian dynamics and referred to as the Caldeira-Leggett model, though its origin can be traced to earlier contributions [1–5].

In previous work [6,7], we explored thermalization in the context of a model where the interaction, both in range and strength, appeared as a generalization of this more familiar Caldeira-Leggett model. Though the earlier context was the sympathetic cooling of atomic gas mixtures, our model was also intended to explore the realm of nonlinearities arising in either, or both, interaction and confining potentials [8]. In particular, plasma physics offers a phenomenological platform to discuss our model as scaling properties, turbulence, strong coupling, and exothermic reactions all play a crucial role.

An intriguing feature reported in Ref. [7] was power-law scaling of the average total interaction energy with total number of particles, for equal number mixtures, as thermalization was approached. Specifically, the scaling exponent was reminiscent of that associated with Kolmogorov scaling associated with turbulent mixing in fluids. Within the explored range of parameters, the scaling was persistent with changing dimensionality of the dynamics. The suggested analogy between turbulent mixing and thermalization originates from the common issue of homogenization. As we show, the interaction energy between the two species transitions from a dynamical regime to one more attuned to a statistical analysis. Thermalization of the two species coincides with the realization of this latter regime, and we interpret this to be the well-mixed state.

In this paper, we explore in more detail this scaling behavior. Aside from exploring a wider range of parameters in our numerical simulations, we construct analytic estimates of the scaling exponents from various thermodynamic perspectives and with variable dimensionality. In one dimension, there do exist conditions under which the exponent does indeed coincide with that seen in Kolmogorov scaling while, under analogous conditions, there are deviations at higher dimensionality. It is worth noting that dimensional arguments behind Kolmogorov scaling are scalar in nature, due to assumptions of isotropy, resulting in an effective one-dimensionality. In our dynamical situation, one-dimensionality favors energy transfer due to the absence of constraints on head-on collisions while, in higher dimensions, angular momentum serves to restrict these, resulting in a slower rate of energy transfer. Also, the scaling becomes extensive in the limit of infinite dimensions, as expected from mean-field constructs and phase-space considerations.

On exploring a broader range of parameters, scaling indicates a saturation in the total interaction energy. This saturation phenomenon occurs when the interaction range is so large that all possible pairwise interactions occur, regardless of the interaction strength. Analogously, saturation also occurs for any interaction range when the interaction strength is so large that either clustering of particles of different species (when their interaction is attractive) or nearly complete spatial separation (when the interaction is repulsive) occurs. The phenomenon is microscopically related to the two-point spatial correlation function between particles of different species. This effect also implies that in a more general setting in which both attractive and repulsive interactions occurs, such as in dense plasmas in the strong-coupling regime, the attractive component dominates over the repulsive component in establishing the dynamics and the total interaction energy. Further

relationships of our work to plasma physics, with particular regard to possible future research directions on anisotropic turbulence and efficient heating protocols, are highlighted in the conclusions.

II. A GENERALIZED INTERACTION MODEL BETWEEN TWO SPECIES

The Hamiltonian we consider is [6–8]

$$H = \sum_{m=1}^{N_A}\left(\frac{P_m^2}{2m_A} + \frac{1}{2}m_A\omega_A^2 Q_m^2\right) + \sum_{n=1}^{N_B}\left(\frac{p_n^2}{2m_B} + \frac{1}{2}m_B\omega_B^2 q_n^2\right) + \gamma\sum_{m=1}^{N_A}\sum_{n=1}^{N_B}\exp\left[-\frac{(Q_m - q_n)^2}{\lambda^2}\right], \quad (1)$$

where (Q_m, P_m) and (q_n, p_n) are the positions and momenta of each particle of the two species A and B, respectively, and positions lie in a generic D-dimensional space. The interspecies term is governed by two parameters, the strength γ and the range λ of the interaction, with the former representing the typical energy exchanged between two distinct particles in a close-distance interaction. Although the interaction Hamiltonian looks rather simple, it allows for the study of a variety of situations, including balanced ($N_A = N_B$) and unbalanced mixtures, attractive ($\gamma < 0$) and repulsive ($\gamma > 0$) interactions, as well as long-range ($\lambda \to \infty$) and short-range interactions. In particular, for a completely unbalanced mixture (for instance, $N_A = 1$ and $N_B \to \infty$), small γ and large interaction range, the model mimics, in the classical limit and for a finite number of particles [9], the genuine Caldeira-Leggett approach used to model dissipation in open systems. It should be noted that we are considering the classical dynamics so reference to Caldeira-Leggett is in terms of the functional form of the interaction. Our choice of a Gaussian form of the interaction term in the Hamiltonian allows for simple analytical estimates based on the canonical ensemble, and therefore in the thermodynamic limit of infinite particle numbers. As first emphasized in Ref. [10], thermalization and equilibration processes are quite insensitive to the microscopic details of the interaction. Therefore we expect our results to be relevant beyond the specific, analytically convenient, interaction term we have adopted.

The equations of motion corresponding to the Hamiltonian in Eq. (1) can be numerically integrated to machine precision. Given the harmonic trapping potential, the initial conditions are drawn from canonical energy distributions consistent with the initial temperatures of the two clouds (see Ref. [7] for details). The time evolution of the particle trajectories, in the presence of interactions, allows us to track the dependence of the total interaction energy on time for typical parameters as shown in Fig. 1. Early on, the interaction energy reflects the periodicity associated with the harmonic trap, while increasing aperiodicity develops with time. For even longer times, the interaction energy settles into a noisy time-averaged value. The inset shows the evolution of the inverse temperatures β_A and β_B of the two subsystems over the same time, with equilibration coinciding with the settling down of the interaction energy. The inverse temperature, as discussed in detail in Ref. [7], is evaluated by looking at the energy variance σ_E^2 where

$$\sigma_E = (\langle E^2\rangle - \langle E\rangle^2)^{1/2} = \sqrt{D}/\beta, \quad (2)$$

where D is the spatial dimensionality, and the averages are taken over the ensemble of particles at any given time. This simple relationship relies on Gibbs-Boltzmann statistics and therefore a weak-coupling approximation [11–13]. The interaction energy is a more robust, coarse-grained indicator whose validity also holds in the strong-coupling limit. More specifically, we have observed situations, for instance, due to strong interspecies repulsion, for which the system does not

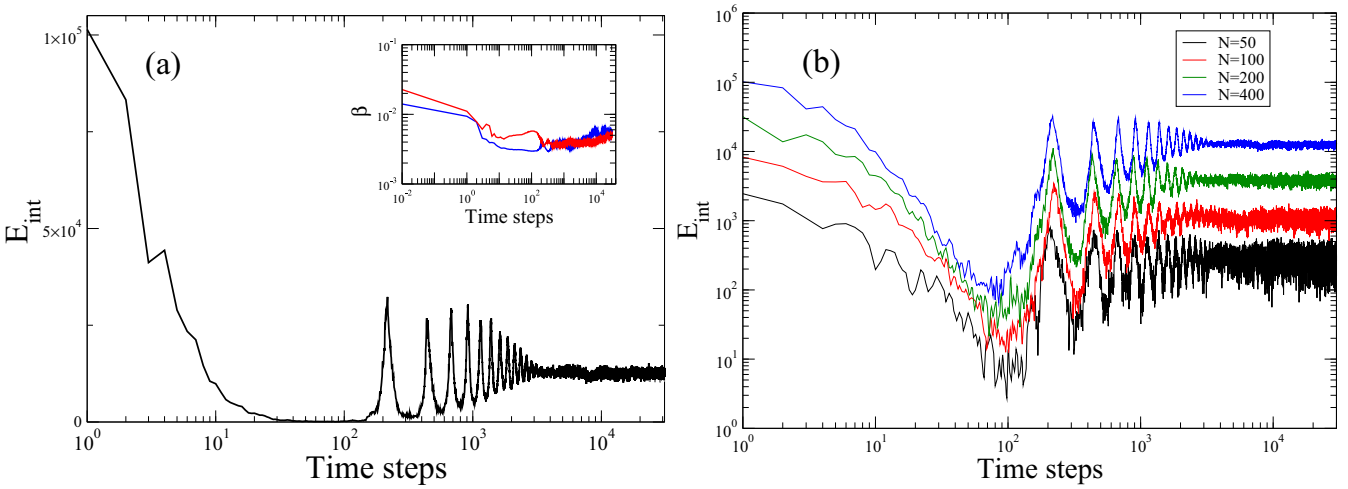

FIG. 1. Left: Plot of the total interaction energy versus time for a given equal number of particles in the two systems. In the inset the inverse temperatures of the two systems are shown versus time, confirming the presence of a regime in which thermalization is assured and showing also the presence of an exothermic equilibration. The simulations were performed with $N_A = N_B = 400$ particles, $\gamma = 20.0$, $\lambda = 0.1$, $\beta_A = 2.0$, $\beta_B = 0.2$, $m_A = m_B = 1.0$, $\omega_A = 1.0$, $\omega_B = 144/89$. Right: Same quantity for varying number of particles in the two systems, qualitatively showing that the interaction energy increases with the number of particles and that its fluctuations after the thermalization stage decrease with the number of particles.

settle into an equilibrium state as defined by a common inverse temperature, yet a stationary situation occurs with different effective inverse temperatures as evaluated from Eq. (2) and a stationary interaction energy. By repeating the numerical simulations for different numbers of particles, we can highlight the scaling behavior seen in the late time-averaged, total interaction energy with respect to the number of particles, reported in Ref. [7]. Note that for the rest of the paper, the term *total interaction energy*, denoted by $\bar{E}_{\rm int}$, will refer to the postsaturation, time-averaged total interaction energy. In the scaling context, the right panel of Fig. 1 notes both the change in this average energy as well as the reduction in fluctuations with increasing particle number. This will prove relevant in determining the accuracy of the power-law scaling results with changing system size.

III. NUMERICAL EXPLORATION

We have numerically evaluated the critical exponents for a range of parameters and for balanced systems with $N = 50, 100, 200, 400, 800$ particles each. The acceptable lower number of particles is determined by the large statistical fluctuations of the interaction energy, while the higher number is limited by the duration of the simulation (requiring about 2 weeks for the largest number of particles, $N = 800$, and 10^5 time steps on a single processor). Although, in many cases, thermalization can occur on shorter timescales, we have decided to standardize the simulations by considering a total duration of 10^5 time steps in all cases. The interaction energy is evaluated by averaging over the last 10^3 time steps of each simulation, where the discussion of the inset plot in the caption of Fig. 2 provides justification for this choice.

In our attempts to improve the precision of the power-law exponent, we have extensively studied its dependence on the run time, the series length of the time-dependent interaction energy used in the time average, as well as the number of particles. The latter is a crucial parameter because we expect that for small number of particles the ergodic hypothesis does not hold on the limited timescales we explore. A manifestation of this can be seen in Fig. 2 where the variation of the time averaged interaction energy with particle number is shown. Deviations from the power-law behavior seen for the smaller N values are a consequence of the absence of ergodicity on the timescales of our simulations. By allowing enough time for thermalization and optimizing the averaging time windows in the thermalization regime, as indicated in the caption for Fig. 2, we obtain the accuracy necessary (relative errors of a few percentages) to validate the predicted behavior for the scaling exponent.

In Fig. 3 we show the scaling of this time-averaged interaction energy, in one dimension, with the number of particles for various γ, corresponding to repulsive and attractive interactions. The values of γ lie between the perturbative case (where thermalization occurs on exceedingly long timescales but there is some analytic tractability) and the strongly coupled case, where any analytical perturbative construction is not expected to hold. On comparing the repulsive and attractive cases in Fig. 3, if all the other parameters are kept equal, then the interaction energy (absolute value) for the attractive case is at least one order of magnitude larger with respect to the repulsive case. This nontrivial feature may be interpreted as due to the different role played by the interaction term in the two cases. The textbook scenario of thermalization consists of two compartments of particles where the interaction (wall between them) is very weak, either due to the interparticle interactions themselves or because the interface between the subsystems is of lower dimensionality as compared with those of the subsystems. The repulsive case follows this scenario. However, this is not a likely scenario for attractive interactions where aggregation or clustering can lead to increased strength in the spatially dependent interactions. Using this notion, the total interaction energy is bounded simply by $E_{\rm int}^{\rm sat} = -\gamma N_A N_B$, when the distance between all pairs $|Q_m - q_n| \ll \lambda$. Including the fact that the particles are moving means that the asymptotic interaction energy seen in the numerics is considerably less (in absolute value). The reduction factor can be estimated, in the case of small λ, by comparing the timescale

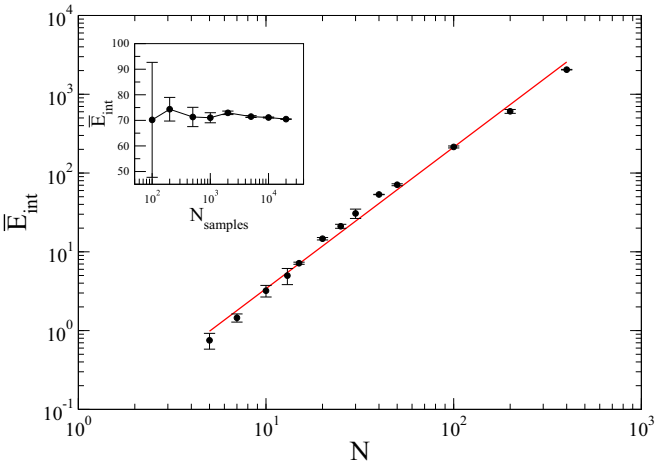

FIG. 2. Total interaction energy $\bar{E}_{\rm int}$ versus the number of particles N, with both quantities shown on logarithmic scales, for a broad range of N encompassing also the few-body case. Deviations from a power-law scaling at small number of particles are attributable to the few-body dynamics which does not allow for meaningful comparison of the time-averaged total interaction energy to the corresponding one obtained by a canonical ensemble average. Including points from the few-body cases does indeed affect the best fit significantly. A scaling exponent $\alpha = 1.80 \pm 0.04$ is obtained for a global fit (red line). Considering only the four rightmost points gives $\alpha = 1.61 \pm 0.04$, while the eight rightmost result in $\alpha = 1.62 \pm 0.02$, showing robustness of the fit for large N. The inset shows the dependence of the standard deviation of the total interaction energy on the number of time steps used for evaluating its average value at the end of the simulation, for the case of $N = 50$ particles. The optimal choice is a compromise between the larger standard deviations for smaller time sequences and the need to avoid bias due to possible residual thermalization dynamics for larger size of the sample. The coupling strength is $\gamma = 2.0$, while the parameters $\lambda, \beta_A, \beta_B, m_A, m_B, \omega_A, \omega_B$ have the same values as in Fig. 1. The error bars in the inset correspond to one standard deviation from the average value, while the errors on the scaling exponent α here and in the following figures are evaluated as one standard deviation in the least-squares analysis. Based on this analysis, we use a minimum of $N = 50$ particles for each species and 10^3 time steps for the time averaging in all other figures.

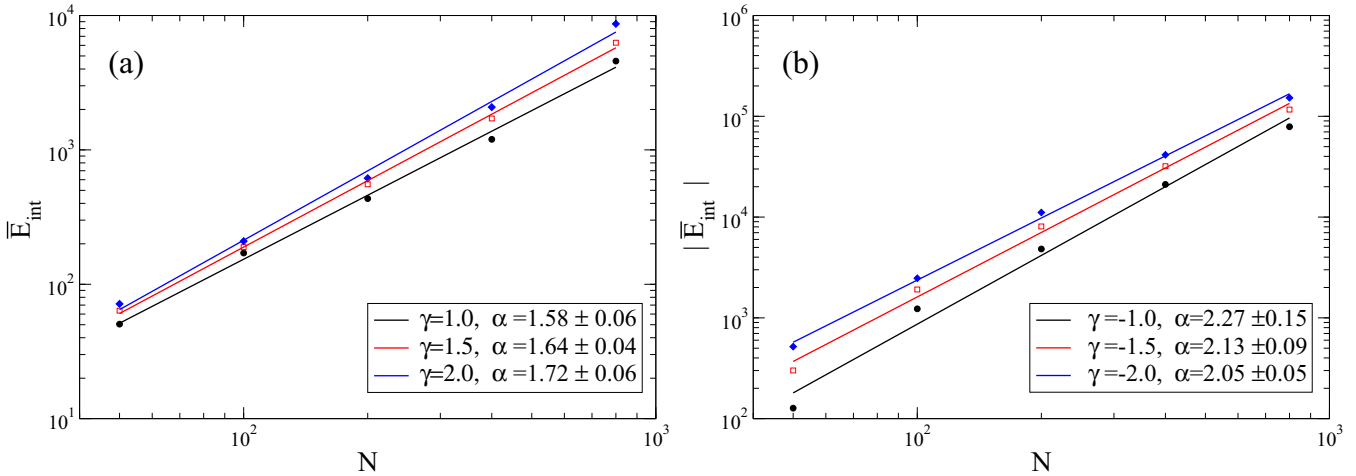

FIG. 3. Scaling of the total interaction energy with system size ($N_A = N_B = N$) for both repulsive (left) and attractive (right) cases. The strength γ is specified while $m_A = m_B = 1.0$, $\lambda = 0.1$, $\omega_A = 1.0$, $\omega_B = 144/89$, $\beta_A = 0.2$, and $\beta_B = 2.0$.

on which the two particles are proximal, i.e., within λ (of order λ/v where v is their relative velocity) with the period of the harmonic oscillation in the trap. For the parameters in Fig. 3, the typical saturation value is about 10 % of $E_{\rm int}^{\rm sat}$.

Also, the attractive case is more efficient, for the same choice of initial conditions, in increasing the total interaction energy of the two systems. The interface between the two systems is more extended in configurational space and there is aggregation rather then phase separation as in the repulsive case. As a consequence, the interactions proceed faster and involve larger clusters of particles. Conversely, as shown by numerical simulations and simple analytical estimates, thermalization in the case of strong repulsion occurs intermittently as it involves small particle numbers at the tails of the already phase-separated clouds. In the attractive case, the thermalization phenomenon can be viewed as proceeding through latent energy stored in the interaction term, which is then released as kinetic and potential energy of each particle. In this sense, it can be viewed as a generalization of Joule-Thompson effects in real gases, with a compression and heating stage rather than the usual expansion and cooling.

The view suggested above is further corroborated by inspecting the total interaction energy at equilibrium, normalized to the coupling strength γ, as a function of γ, shown in Fig. 4. The interaction energy saturates both at large values of γ due to species separation for repulsive interactions, at a small value for $E_{\rm int}$, and at large negative values of γ due to species clustering, with a large absolute value of $E_{\rm int}$. As discussed in Ref. [7], the interaction energy is a macroscopic indicator of the ensemble-averaged distance between two different species particles, as

$$\langle (q_n - Q_m)^2 \rangle = -\lambda^2 \ln\left(\frac{\langle E_{\rm int}\rangle}{\gamma N_A N_B}\right). \tag{3}$$

In Fig. 4 there is an intermediate region of values of γ where these appears to be a crossover between the two extreme values. As we will describe, this is where the considerations of the analytical model we develop may apply. It would appear that special care is required in the limit as γ approaches zero, as the interaction energy is zero by definition in the limit. The numerical analysis has been repeated in higher dimensions, confirming the general trend with some distinguishing features. For the same parameters, higher dimensions show ever smaller interaction energy, as the particles may dilute in a progressively larger phase space. Also, the presence of angular momentum allows for evasive trajectories which are forbidden in the one-dimensional case. The difference between attractive and repulsive interactions is amplified by higher dimensionality, and in the full three-dimensional (3D) case the asymptotic values of the interaction energies differ by about three orders of magnitude, in contrast to a single order of magnitude for the 1D case.

A second prominent feature in comparing the attractive and repulsive cases in Fig. 3 is that the scaling exponent is compatible with $\alpha = 2$ within two standard deviations for the attractive case and instead assumes values significantly

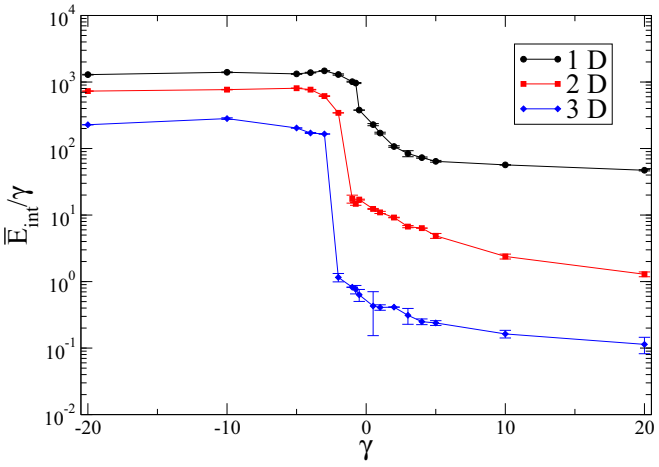

FIG. 4. Total interaction energy at thermal equilibrium per unit of coupling strength γ versus the coupling strength itself for baths made of 10^2 particles each, and the same temperatures and interaction range as in Fig. 3. The plots show evidence of the saturation of the interaction energy in both extremes of strong attractive and repulsive couplings in all dimensions.

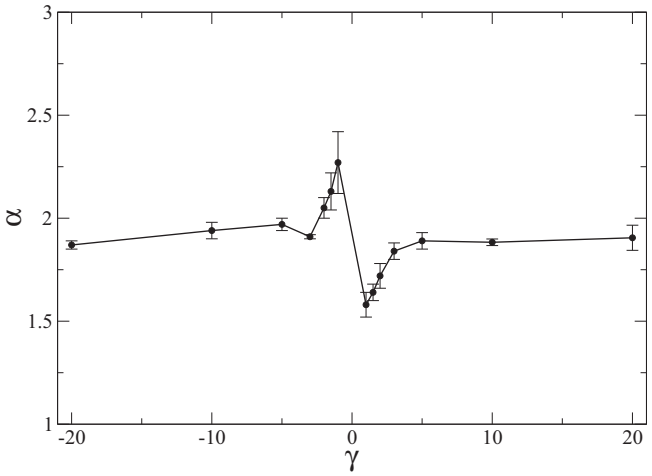

FIG. 5. Scaling exponent α versus the coupling strength γ for the same temperatures and interaction range as in Fig. 4 in the 1D case. A narrow region at small values of γ is visible in which anomalous scaling occurs. Notice that the error bars in the region of small and negative γ are large enough to make the values compatible with $\alpha = 2$ within three standard deviations at most, while the case of anomalous scaling is statistically much stronger for positive values of γ. Specifically, for our data, at $\gamma = 1$ we get $\alpha = 1.58 \pm 0.06$ which is about 1.3 standard deviations from the theoretically expected value 5/3 discussed in the analytical section. The analysis has been repeated for the case of 2D and 3D systems at different coupling strengths and all the other parameters kept constant as in the 1D case, obtaining exponents of $\alpha = 1.85 \pm 0.02$ ($\gamma = 1$), $\alpha = 1.74 \pm 0.05$ ($\gamma = 2$), $\alpha = 1.82 \pm 0.04$ ($\gamma = 20$), for the 2D case, and $\alpha = 2.03 \pm 0.04$ ($\gamma = 1$), $\alpha = 2.03 \pm 0.04$ ($\gamma = 2$), $\alpha = 2.26 \pm 0.12$ ($\gamma = 20$), for the 3D case. A comprehensive analysis of anomalous scaling for the higher-dimensionality cases will be the subject of future investigation, including the case of anisotropic trapping.

lower in the repulsive case. This suggests the consideration of a broader range of γ values (as in Fig. 4). The resulting dependence of the scaling exponent on coupling strength γ is shown in Fig. 5. At large absolute values of γ the scaling exponent is compatible with 2. In this highly nonperturbative regime, as noted above, the particles are strongly clustered in the attractive case, and they all interact with each other. In the repulsive case there is species separation so we expect only intermittent interactions by particles at the boundary between the two separated species. This constitutes a small subset of each species, and as discussed above the interaction energy should therefore scale with the square of the particle number (for a balanced mixture) times a suppression factor proportional to the thickness of the boundary region with respect to the interaction range λ. In the weakly interacting regime, the scaling exponent is in line with the expectations of homogeneity and Kolmogorov-like mixing as discussed in the next section. By contrast, at large γ, the strong interparticle interaction is analogous to a high viscosity regime in fluids, which precludes turbulence and the associated scaling. Once again, the trend is confirmed in higher-dimensional cases, as indicated by the data discussed in the caption of Fig. 5.

IV. ANALYTICAL CONSIDERATIONS

It turns out that much of the behavior seen can be recovered using equilibrium statistical mechanics and thermodynamics considerations. We begin by rewriting the Hamiltonian Eq. (1) as the sum of the free and interaction Hamiltonians, respectively, $H = H_0 + H_{\rm int}$. Having in mind weak-coupling, perturbative expansions, we make explicit the interaction strength γ in the interaction Hamiltonian, such that $H_{\rm int} = \gamma I$, where I is a dimensionless quantity. The corresponding partition function and the expectation value of energy at thermal equilibrium corresponding to inverse temperature β are, respectively,

$$Z = \int \prod_{m=1}^{N_A} d\vec{Q}_m d\vec{P}_m \prod_{n=1}^{N_B} d\vec{q}_n d\vec{p}_n \exp\left[-\beta(H_0 + \gamma I)\right], \quad (4)$$

$$\langle E \rangle = -\frac{1}{Z}\frac{\partial Z}{\partial \beta} = \frac{1}{Z}\int \prod_{m=1}^{N_A} d\vec{Q}_m d\vec{P}_m \prod_{n=1}^{N_B} d\vec{q}_n d\vec{p}_n \times (H_0 + \gamma I)\exp[-\beta(H_0 + \gamma I)]. \quad (5)$$

We expand the expression for the energy in terms of the coupling strength γ, to obtain

$$\langle E \rangle = \frac{D(N_A + N_B)}{\beta} + \gamma F_D(\rho_A, \rho_B) N_A N_B, \quad (6)$$

where we have introduced a form factor $F_D(\rho_A, \rho_B)$, defined as

$$F_D(\rho_A, \rho_B) = \left(1 + \rho_A^2 + \rho_B^2\right)^{-\frac{D}{2}}\left[D + 1 - \frac{D}{2}\frac{\rho_A^{-2}\left(1 + \rho_A^{-2}\right) + \rho_B^{-2}\left(1 + \rho_B^{-2}\right)}{\left(1 + \rho_A^{-2}\right)\left(1 + \rho_B^{-2}\right) - 1}\right]. \quad (7)$$

Here $\rho_A = \xi_A/\lambda$, $\rho_B = \xi_B/\lambda$, where $\xi_A = \sqrt{2/\beta m_A \omega_A^2}$ and $\xi_B = \sqrt{2/\beta m_B \omega_B^2}$ are the thermal lengths of the two species. The analysis can be simplified by assuming that both species have equal mass and, hence, identical frequencies in the harmonic trap, which implies $\xi_A = \xi_B = \xi$ corresponding to the inverse equilibrium temperature β. The form factor can also be re-expressed contrasting β with β_λ defined as $\beta_\lambda = 2/(m\omega^2\lambda^2)$, which corresponds to $\xi = \lambda$.

Figure 6 shows the variation of the form factor with changing β normalized to β_λ. We can now differentiate behavior according to the importance of these thermal lengths with respect to the interaction range, obtaining approximate analytical expressions for the different regimes visible in Fig. 6. This is facilitated by considering the expression for F_D when $\rho_A = \rho_B = \rho$:

$$F_D(\rho) = \frac{\rho^{-2}(1 + 2\rho^2)^{-\frac{D}{2}}(D + 2 + \rho^{-2})}{(1 + \rho^{-2})^2 - 1}. \quad (8)$$

In the limit of $\lambda \gg \xi$, or, equivalently, $\rho \to 0$, $F_D \to 1$ and the average total energy at equilibrium becomes

$$\langle E \rangle = \frac{D(N_A + N_B)}{\beta} + \gamma N_A N_B. \quad (9)$$

In this limit we recover the behavior of the Caldeira-Leggett model. In particular, for the specific setting in which

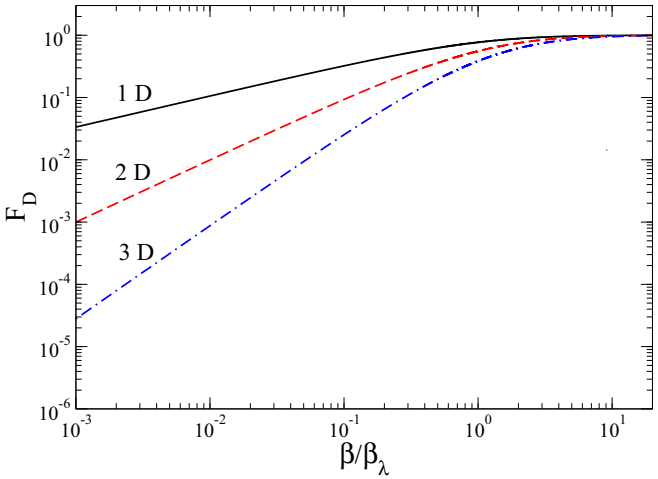

FIG. 6. Form factor F_D versus the inverse temperature β normalized to the interaction range inverse temperature β_λ.

the model is usually applied, with one of the two species playing the role of a large reservoir (for instance, if $N_A \gg N_B$), the total energy becomes extensive, while being dependent on N^2 in the case of a balanced mixture ($N_A = N_B = N$). The latter result is consistent with the idea that long range interactions are not extensive, as there will be N^2 distinct interparticle interaction energy terms.

We now consider the situation where the thermal lengths are much larger than the interaction range, that is, $\lambda \ll \xi$ ($\rho \gg 1$). In this regime the form factor F_D depends on temperature, as seen in Fig. 6, and may be approximated as $F_D \simeq (1 + D/2)(2\rho^2)^{-D/2}$, with the corresponding expression for the average total energy

$$\langle E\rangle \simeq \frac{D(N_A+N_B)}{\beta} + \gamma\left(1+\frac{D}{2}\right)\left(\frac{\beta}{2\beta_\lambda}\right)^{\frac{D}{2}} N_A N_B. \quad (10)$$

In the 1D case and balanced mixtures ($N_A = N_B = N$), the average total energy

$$\langle E\rangle \simeq \frac{2N}{\beta} + \gamma\frac{3N^2}{2\sqrt{2}}\frac{\lambda}{\xi} = \frac{2N}{\beta} + \gamma\frac{3N^2}{2\sqrt{2}}\left(\frac{\beta}{\beta_\lambda}\right)^{1/2}. \quad (11)$$

The two terms constituting the average total energy depend linearly and quadratically on the number of particles, respectively. We now impose a "generalized extensivity" property such that $\langle E\rangle$ scales as N^α, where the exponent α should lie between the genuine extensive case of $\alpha = 1$ achieved in the noninteracting case and $\alpha = 2$ reached in the strong-coupling limit of $\gamma \to \pm\infty$. This homogeneity in the two contributions to the total energy is achieved if the inverse temperature itself depends on N with a power-law exponent, more precisely if $\beta \propto N^{-\tau}$. Then the two terms on the right-hand side will depend on $N^{1+\tau}$ and $N^{2-\tau/2}$, respectively. The request for homogeneity is fulfilled if $\tau = 2/3$. The average total interaction energy then will scale as $\langle E_{\rm int}\rangle \sim N^{5/3}$, i.e., $\alpha = 5/3$. The evaluation of the scaling exponent is readily extended to D dimensions, based on the second term of the right-hand side of Eq. (10) and, using the same reasoning as above, we find the scaling exponent to depend on dimensionality as

$$\alpha = \frac{D+4}{D+2}. \quad (12)$$

This means $\alpha = 5/3, 3/2, 7/5$ in 1D, 2D, and 3D, respectively. It is worth noting that the extensive case is obtained in the limit of infinite dimensions and that quadratic scaling corresponds to a zero-dimensional system. In order to compare these expectations with numerical simulations, one should add, on top of the request for a Maxwell-Boltzmann distribution (which implies a sort of weak-coupling limit, with small values of γ) also the ergodic theorem in which the ensemble averages evaluated above are matched by time-averaged quantities. This is a requirement for thermal equilibration, as discussed in Ref. [8].

The scaling argument provided above may be considered as a necessary, but not sufficient, condition for the stability of the system. More insights on the stability with respect to the sign and the magnitude of the interaction strength γ may be arrived at by thermodynamic considerations. In a stable thermodynamic system the entropy is a concave function of energy [14], which is always satisfied if the heat capacity is positive valued. In our case the heat capacity for short-range interactions, where K_B is the Boltzmann constant, is

$$C = \frac{d\langle E\rangle}{dT} = DK_B \times\left[N_A+N_B-\frac{\beta\gamma}{2}\left(1+\frac{D}{2}\right)\left(\frac{\beta}{2\beta_\lambda}\right)^{D/2} N_A N_B\right]. \quad (13)$$

A change in the sign of the curvature in the entropy is indicative of a drastic change in the dynamical behavior, a sort of phase transition. When the interaction is attractive ($\gamma < 0$) the heat capacity is always positive. However, for a repulsive interaction ($\gamma > 0$) there exists a critical inverse temperature above which the system is unstable. This threshold is given by

$$\beta_{\rm crit} = 2\left[\beta_\lambda\gamma\left(1+\frac{D}{2}\right)\frac{N_A N_B}{N_A+N_B}\right]^{\frac{-2}{D+2}}\beta_\lambda. \quad (14)$$

The existence of a threshold can be simply understood by inspecting the motion of two generic interacting particles in the 1D case. Below the critical inverse temperature, both particles are free to explore the entire trap while, at lower temperatures, each particle is confined on one side of the trap. This can be thought of in terms of a phase separation which diminishes the interaction energy contribution and the overall scaling with the number of particles, in analogy to the discussion appeared in Sec. III of Ref. [6] in terms of stability analysis. At the critical inverse temperature and for an unbalanced mixture, the total interaction energy is given by

$$\langle E_{\rm int}\rangle \sim \gamma^{2/(D+2)}(N_A N_B)^{2/(D+2)}(N_A+N_B)^{D/(D+2)}, \quad (15)$$

which obviously becomes extensive in one of the two systems when the other is composed of just one particle. For balanced mixtures, the scaling confirms what was shown earlier, namely $\langle E_{\rm int}\rangle \sim N^{\frac{D+4}{D+2}}$. We note that for our parameters (which involve balanced mixtures), the critical values fall within the inverse temperatures we consider for the two species. Further,

we stress that the estimate is valid only in the thermodynamic (large particle number) limit and that we expect deviations given the small number of particles we consider.

In relation to an earlier comment on Fig. 4 about the ratio of the interaction energy divided by γ in the limit $\gamma \to 0$, we need to extend the scaling relation (in N) to include the effects of γ and λ. The equilibrium temperature reached can be reasonably expected to depend on the strength γ and the range λ of the interaction. In keeping with the earlier analysis, we consider $T \propto N^{\alpha}\gamma^{\delta}\lambda^{\eta}$ and, using analogous dimensional arguments, it can be shown that $\alpha = \delta = 2/(D+2)$ while $\eta = 2D/(D+2)$. Thus, for fixed N and λ, the interaction energy scales as $\gamma^{1-\beta D/2} = \gamma^{2/(D+2)}$ [consistent with Eq. (15) derived from independent considerations] or $\gamma^{2/3}$ in one dimension. This clearly indicates that the interaction energy goes to 0 as γ approaches 0 from either direction while the ratio shown in Fig. 4 is ill defined as $\gamma \to 0$.

V. CONCLUDING REMARKS

We have elaborated on scaling behavior, first reported in Ref. [7], seen in the interaction energy, of a binary mixture with short-range interactions, with respect to system size, at the onset of thermalization. Contrasting extensive numerical simulations with analytic constructs we find that the scaling exponent that coincides with the one seen in turbulent mixing occurs only for small positive values of the interaction coupling strength. This is the regime where the interspecies interaction can be considered as a small perturbation with respect to the external harmonic potential experienced by both species. The scaling behaviors in other parameter regimes are more readily anticipated using simple analytic arguments. It should be noted that scaling is also expected to break down when using nonlinear trapping potentials, where thermalization itself is also more involved, as discussed in Ref. [8].

Our results may have relevance in a variety of many-body physics contexts, including ultracold atomic physics where the turbulent cascade of energy has been recently studied both theoretically [15] and experimentally [16], requiring extension of our model to the quantum realm. Although plasmas contain both intraspecies and interspecies interactions, the interplay among strong coupling, scaling behavior, and turbulence discussed here may be of interest in the context of extremely exothermic systems such as magnetically confined fusion plasmas. Features of plasmas can be isolated and simulated, in the spirit of the numerical studies for evaluating nuclear reaction rates reported in Ref. [17]. In particular, the relationship between Kolmogorov scaling and effective dimensionality of confinement is crucial in magnetized fluids [18–21], and we plan to analyze scaling features in the general case of anisotropic harmonic trapping. Our model is also relevant to study efficient and fast heating, for instance, transferring to the plasma physics context techniques developed for fast cooling in ultracold atomic physics [22–26]. Additionally, the Caldeira-Leggett model has been shown to share similarities with the linearized Vlasov-Poisson equation, including the presence of an analog of Landau damping [27]. Our generalization of the Caldeira-Leggett model to a nonperturbative setting should allow for the exploration of this analogy in a fully nonlinear regime, which is presumably more appropriate for the description of plasma dynamics.

[1] V. B. Magalinskii, Sov. Phys. JETP **9**, 1381 (1959).
[2] P. Ullersma, Physica **32**, 27 (1966); **32**, 56 (1966); **32**, 74 (1966); **32**, 90 (1966).
[3] A. O. Caldeira and A. J. Leggett, Phys. Rev. Lett. **46**, 211 (1981).
[4] A. O. Caldeira and A. J. Leggett, Ann. Phys. **149**, 374 (1983).
[5] A. O. Caldeira and A. J. Leggett, Phys. Rev. A **31**, 1059 (1985).
[6] R. Onofrio and B. Sundaram, Phys. Rev. A **92**, 033422 (2015).
[7] F. Jauffred, R. Onofrio, and B. Sundaram, J. Phys. B **50**, 135005 (2017).
[8] F. Jauffred, R. Onofrio, and B. Sundaram, Phys. Lett. A **381**, 2783 (2017).
[9] S. T. Smith and R. Onofrio, Eur. Phys. J. B **61**, 271 (2008).
[10] A. I. Khinchin, *Mathematical Foundations of Statistical Mechanics* (Dover, New York, 1949).
[11] E. W. Montroll and K. E. Shuler, J. Chem. Phys. **26**, 454 (1957).
[12] K. Andersen and K. E. Shuler, J. Chem. Phys. **40**, 633 (1964).
[13] H. C. Andersen, I. Oppenheim, K. E. Shuler, and G. H. Weiss, J. Math. Phys. **5**, 522 (1964).
[14] J. Naudts, J. Phys.: Conf. Ser. **201**, 012003 (2010).
[15] A. S. Bradley and B. P. Anderson, Phys. Rev. X **2**, 041001 (2012).
[16] N. Navon, A. L. Gaunt, R. P. Smith, and Z. Hadzibabic, Nature **539**, 72 (2016).
[17] D. H. E. Dubin, Phys. Plasmas **15**, 055705 (2008).
[18] R. H. Kraichnan, Phys. Fluids **8**, 1385 (1965).
[19] G. Y. Antar, Phys. Rev. Lett. **91**, 055002 (2003).
[20] J. Mason, F. Cattaneo, and S. Boldyrev, Phys. Rev. Lett. **97**, 255002 (2006).
[21] J. C. Perez, J. Mason, S. Boldyrev, and F. Cattaneo, Phys. Rev. X **2**, 041005 (2012).
[22] X. Chen, A. Ruschhaupt, S. Schmidt, A. del Campo, D. Guéry-Odelin, and J. G. Muga, Phys. Rev. Lett. **104**, 063002 (2010).
[23] S. Choi, R. Onofrio, and B. Sundaram, Phys. Rev. A **84**, 051601(R) (2011).
[24] J.-F. Schaff, P. Capuzzi, G. Labeyrie, and P. Vignolo, New. J. Phys. **13**, 113017 (2011).
[25] R. Onofrio, Phys. Uspekhi **59**, 1129 (2016).
[26] P. Diao, S. Deng, F. Li, S. Yu, A. Chenu, A. del Campo, and H. Wu, New. J. Phys. **20**, 105004 (2018).
[27] G. I. Hagstrom and P. J. Morrison, Physica D **240**, 1652 (2011).